Molecular Analysis of Secondary Organic Aerosol and Brown Carbon from the Oxidation of Indole

Feng Jiang[1,2*], *Kyla Siemens*[3], *Claudia Linke*[1], *Yanxia Li*[1], *Yiwei Gong*[1], *Thomas Leisner*[1,5], *Alexander Laskin*[3,4], *and Harald Saathoff*[1*]

[1]Institute of Meteorology and Climate Research, Karlsruhe Institute of Technology, 76344 Eggenstein–Leopoldshafen, Germany
[2]Institute of Applied Geosciences, Working Group for Environmental Mineralogy and Environmental System Analysis, Karlsruhe Institute of Technology, 76131 Karlsruhe, Germany
[3]Department of Chemistry, Purdue University, West Lafayette, Indiana 47907, United States
[4]Department of Earth, Atmospheric and Planetary Sciences, Purdue University, West Lafayette, Indiana 47907, United States
[5]Institute of Environmental Physics, Heidelberg University, 69120 Heidelberg, Germany

Correspondence to: Feng Jiang (feng.jiang@kit.edu) and Harald Saathoff (harald.saathoff@kit.edu)

Abstract. Indole (*ind*) is a nitrogen-containing heterocyclic volatile organic compound commonly emitted from animal husbandry and from different plants like maize with global emissions of 0.1 Tg y^{-1}. The chemical composition and optical properties of indole secondary organic aerosol (SOA) and brown carbon (BrC) are still not well understood. To address this, environmental chamber experiments were conducted to investigate the oxidation of indole at atmospherically relevant concentrations of selected oxidants (OH radicals and O_3) with/without NO_2. In the presence of NO_2, the SOA yields decreased by more than a factor of two but the mass absorption coefficient at 365 nm (MAC_{365}) of *ind*-SOA was 4.3 ± 0.4 m^2 g^{-1}, which was 5 times higher than that in experiments without NO_2. In the presence of NO_2, $C_8H_6N_2O_2$ (identified as 3-nitroindole) contributed 76% to the all organic compounds detected by a chemical ionization mass spectrometer, contributing ~50% of the light absorption at 365 nm (Abs_{365}). In the absence of NO_2, the dominating chromophore was $C_8H_7O_3N$ contributing to 20–30% of Abs_{365}. Indole contributes substantially to the formation of secondary BrC and its potential impact on the atmospheric radiative transfer is further enhanced in the presence of NO_2, as it significantly increases the specific light absorption of *ind*-SOA by facilitating the formation of 3-nitroindole. This work provides new insights into an important process of brown carbon formation by interaction of two pollutants, NO_2 and indole, mainly emitted by anthropogenic activities.

1. Introduction

Secondary organic aerosol (SOA) is generated by atmospheric oxidation of biogenic and anthropogenic volatile organic compounds (VOCs), and it has a profound impact on air quality, visibility, human health, and climate (Shrivastava et al., 2017; Hallquist et al., 2009). SOA is generally considered as poorly absorbing and predominantly light-scattering material that leads to atmospheric cooling. However, there are colored SOA compounds, known as brown carbon (BrC), which absorb solar radiation in the near-ultraviolet (UV) and visible spectral range contributing to warming effects (Moise et al., 2015; Laskin et al., 2015). BrC has a significant impact on climate forcing, accounting for 7%–19% of the light absorption by aerosols as estimated by global modeling study of Feng et al. (2013). In addition, Zeng et al. (2022) found that different geographic areas BrC can account for ~ 7–48% of the direct radiative forcing caused by both BrC and black carbon (BC).

Sources of BrC are mainly attributed to primary emission from biomass burning and fossil fuel combustion (Andreae and Gelencser, 2006), complemented by secondary BrC compounds formed in the atmosphere as aged SOA of biogenic and anthropogenic origin (Xie et al., 2017; Laskin et al., 2014). Various studies have explored SOA and BrC from oxidation of aromatic VOCs, such as ethylbenzene (Yang et al., 2022), toluene (Lin et al., 2015; Li et al., 2021b), and naphthalene (Siemens et al., 2022; He et al., 2022). However, only a few investigations have examined SOA and BrC from oxidation of heterocyclic VOCs (Mayorga et al., 2022; Jiang et al., 2019; Montoya-Aguilera et al., 2017).

Indole, an important nitrogen-containing heterocyclic compound composed of fused benzene and pyrrole rings, is a significant VOC in the atmosphere. There are various natural and anthropogenic sources for atmospheric indole, including biomass burning (Laskin et al., 2009), animal husbandry (Yuan et al., 2017), agriculture plants like maize or rice (Erb et al., 2015; Skoczek et al., 2017), and tea manufacturing processes (Zeng et al., 2016). Global emissions and emission factors of indole are around 0.1 Tg y^{-1} and 0.6 ug m^{-2} h^{-1}, respectively (Misztal et al., 2015). This is already half of emissions of one of the most abundant amines, trimethylamine, with about 0.2 Tg y^{-1} for global emissions (Yu and Luo, 2014). At selected locations, indole mixing ratios can reach around 1–2.7 ppb at daytime and 1.5–3.7 ppb at nighttime, which is around 10 times higher than isoprene levels during a spring flowering event at nighttime (Gentner et al., 2014). Despite its significant presence in the atmosphere, there are very limited studies investigating the formation of SOA and BrC from atmospheric oxidation of indole (referred to as *ind*-SOA hereafter).

An early study by Atkinson et al. (1995) investigated the gas-phase rate constants of indole with different oxidants. The study reported high rate constants for reactions of indole with hydroxyl (OH) and nitrate (NO_3) radicals [$(1.54 \pm 0.35) \times 10^{-10}$ and $(1.3 \pm 0.5) \times 10^{-10}$ cm^3 $molecule^{-1}$ s^{-1}], respectively, while the reaction with ozone is much slower $(4.9 \pm 1.8) \times 10^{-17}$ cm^3 $molecule^{-1}$ s^{-1} (Atkinson et al., 1995). A more recent study reported that the addition of OH radicals was the dominant pathway for indole reactions with N-(2-formylphenyl)formamide ($C_8H_7O_2N$) being an important product (Xue et al., 2022).

Environmental chamber experiments were conducted to study *ind*-SOA and its BrC components (Montoya-Aguilera et al., 2017; Baboomian et al., 2023). The SOA yield and mass absorption coefficient at 300 nm (MAC_{300nm}) of *ind*-SOA were reported as 1.3 ± 0.3 and ~ 2 m^2 g^{-1}, respectively. The absorption Ångström exponent (*AAE*) of *ind*-SOA were 6.8 ± 0.2 at 375–550 nm and 5.83 ± 0.3 at 315–450 nm, respectively (Li et al., 2021a). The major monomer components of *ind*-SOA were identified as $C_8H_7O_3N$, isatin ($C_8H_5O_2N$), and isatoic anhydride ($C_8H_5O_3N$), while

tryptanthrin ($C_{15}H_{10}O_2N_2$) and indigo dye ($C_{16}H_{10}O_2N_2$) were the most abundant dimers (Montoya-Aguilera et al., 2017). Notably, nitroindole ($C_8H_6N_2O_2$) was one of the strongest chromophores in *ind*-SOA, produced in high abundance through both NO_3 radicals and OH radical oxidation in the presence of NOx (Baboomian et al., 2023). However, the chemical composition, formation mechanism, and optical properties of *ind*-SOA including its BrC components formed at atmospherically relevant conditions remain poorly understood.

In this study, we conducted simulation chamber experiments to investigate the chemical composition, formation mechanism, and optical properties of *ind*-SOA. The experiments were performed by ozonolysis and subsequent OH radical oxidation of indole at three simulated atmospheric conditions: a reference case of indole oxidation (REF), *ind*-SOA formed in presence of ammonium sulfate seed particles (AS); and *ind*-SOA formed in presence of both AS seed and NO_2 (AS-NO_2). We identified the major oxidized products of *ind*-SOA from the three experiments, measured its optical properties, and examine how NO_2 influences the atmospheric oxidation mechanisms leading to the formation of BrC chromophores.

2. Experimental methods

2.1. Particle generation and sampling

Experiments were conducted in the Aerosol Interaction and Dynamics in the Atmosphere (AIDA) simulation chamber operated at dark conditions, at relative humidity (RH) of ~30%, and at room temperature (~30 ºC), as shown in Table 1. The core measurement instrumentation used in this work is shown in Fig. S1. The detailed description of the AIDA chamber, its operation modes, and the associated measurement techniques were published elsewhere (Gao et al., 2022; Saathoff et al., 2009). Briefly, *ind*-SOA was produced from ozonolysis of indole in the presence/absence of NO_2 and $(NH_4)_2SO_4$ seed particles, with experiment-specific conditions listed in Table 1. For the REF experiment (Fig. S2a), indole (≥ 99% purity, Sigma-Aldrich) was dissolved in in toluene (>99.9% p.a. grade, Merk). The solution was used to generate an indole coating on a glass tube of 1.5 m length and 40 mm diameter by evaporating the toluene in the rotating tube. The ~~methanol (HPLC grade, Honeywell) and the methanol/~~indole ~~mixture~~ was evaporated into the AIDA chamber with a flow of 0.01 m^3 min^{-1} of synthetic air through the coated tube for 2-3 hours obtaining indole mass concentrations of ~~to obtain~~ 90–150 µ~~u~~g m^{-3} ~~of indole mass concentrations (Montoya Aguilera et al., 2017)~~. The ozonolysis was started by adding 600–800 ppb of O_3. 2,3-dimethyl-2-butene (TME) was later injected and reacted~~mixed~~ with the excess of O_3 to form OH radicals (Lambe et al., 2007)~~;~~. For comparable levels of ozone and TME in the AIDA chamber, Salo et al., 2011, calculated OH radical levels of 0.2–1.0×10^7 molecules cm^{-3} employing the Master Chemical Mechanism 3.1 (Bloss et al., 2005). ~~for which calculated concentrations were 0.2–1.0×10^7 molecules cm^{-3} (Salo et al., 2011).~~ Following injection of OH radicals, rapid growth of *ind*-SOA was observed in each of the experiments. To reduce the wall loss effect on *ind*-SOA formation, we inject ammonium sulfate (AS) seed particles. In these experiments (Fig. S2b and c), ammonium sulfate (Merck, 99.5%) in ultra-pure water was aerosolized using an ultrasonic nebulizer (Synaptec), introduced into the AIDA chamber to reach mass loading of ~50 ug m^{-3} (Fig. S2b and c), before injecting indole. The number concentration and mobility mode size of the AS seed particles were ~2000 cm^{-3} and ~230 nm, respectively. For NO_2-containing experiments referred as AS-NO_2 (Fig. S2c), NO_2 (99.5% purity, Basi Schöberl GmbH) was injected into the chamber to reach ~ 60 ppb after finishing indole injection, followed

by adding 100 ppb of O_3. However, indole was oxidized slowly in AS-NO_2 experiments, compared to REF and AS conditions. After 30 minutes, the products were further oxidized by adding more O_3 and TME. Please note that the difference of adding O_3 in AS-NO_2 experiments, compared with REF and AS experiments, was to investigate the reaction of indole with NO_3 radicals. However, this will not be discussed in this manuscript. The concentrations of O_3 and NO_2 in the chamber were recorded in real time by a gas monitor ($O_3$41M & AS32M, Environment S.A). Before starting experiments, the background samples from the AIDA chamber were collected on the filters. Compared to sample filters, the absorption of background filters from 240 nm to 800 nm only accounted for 1%. Background measurements for both the gas and particle phase were performed before and after the first addition of indole to identify any contamination inside the chamber. The gas background levels were almost negligible for all experiments. For measurements by the chemical ionization mass spectrometer, most of the particle background signals were from filter matrix contaminations mainly due to fluorinated constituents. We subtracted the mass spectra of the background filter samples from those of the particle-loaded filter samples for the same experiments. This procedure has been described by Gao et al., (2022). After the mass concentrations of *ind*-SOA became stable inside the chamber, the aerosol samples were collected onto one Teflon filter (polytetrafluorethylene (PTFE), 1 µm, SKC Inc) and two parallel quartz filters (47 mm diameter, Whatman) for each experiment (Fig. S2).

2.2. Online measurement instrumentations

The particle number size distributions were monitored by a scanning mobility particle sizer (SMPS) containing a differential mobility analyzer (DMA; 3071, TSI Inc.) connected to a condensation particle counter (CPC, 2772, TSI Inc.). In addition, particle number concentrations were measured by CPC (3022a, TSI Inc.). SMPS and CPC data analysis was also shown in a previous study (Gao et al., 2022). The chemical composition and aerodynamic size of *ind*-SOA were characterized by a high-resolution time-of-flight aerosol mass spectrometer (HR-ToF-AMS, Aerodyne Inc. hereafter AMS). Details about AMS calibration and data processing are included in the supplemental information (Sect. 1). The effective density (ρ_{eff}) was derived from the measurement of the vacuum aerodynamic diameter (d_{va}) obtained by AMS and the mobility equivalent diameter (d_m), see figures S11 and S12 (Kostenidou et al., 2007), as shown in the supplemental information (Sect. 3). The indole concentration and lowly oxygenated gaseous oxidation products were measured by a proton-transfer reaction time-of-flight mass spectrometer (PTR-ToF-MS 4000, Ionicon Analytic GmbH), with specific details provided in the supplemental information (Sect. 2). The SOA yields (Y_{SOA}) were calculated as $Y_{SOA}=\Delta SOA/\Delta VOC$, where ΔSOA values were inferred from the SMPS measurements and ΔVOC were measured by PTR-ToF-MS (see the supplemental information, Sect. 4). The detailed information about the wall loss calculation is shown in Sect. 5 in the supplement. During relatively short experimental time of <200 min and due to the large size of the simulation chamber, particle losses contributed typically 4% or less to the total SOA mass. In the presence of AS seed particles, the gas loss decreased by ~6 times. Since the wall losses of particles and trace gases were relatively low, we did not correct the gas and particle concentrations. Additionally, highly oxygenated gaseous oxidation products were measured with a filter inlet for gases and aerosols coupled to a high-resolution time-of-flight chemical ionization mass spectrometer (FIGAERO-HR-ToF-CIMS, Aerodyne Research Inc. hereafter CIMS) employing iodide (I^-) as the reagent ion.

2.3. Determination of optical properties of *ind*-SOA

Online analysis of the *ind*-SOA optical properties was performed using a photoacoustic spectrometer (PAS) operating at three wavelengths (405, 520, and 658 nm) (Linke et al., 2016). The mass absorption coefficient (*MAC*) was calculated as

$$MAC_{online}(\lambda) = \frac{\alpha(\lambda)}{C_{SOA}} \quad (1)$$

Where the α (Mm^{-1}) absorption is measured by PAS, and the C_{SOA} (μg m^{-3}) is the SOA mass loading inferred from SMPS measurements.

Offline optical measurements were performed using Aqualog fluorometer (HORIBA Scientific, USA), which gives light absorption and excitation-emission spectra. Methanol soluble organic carbon (MSOC) was extracted from one quartz filter in each experiment with 5 mL of methanol (HPLC, Honeywell) using ultrasound sonication for 30 min. Please note that we used methanol and also acetonitrile (see next section) to extract the filter samples as to achieve comparability with previous work i.e. by Montoya-Aguilera et al. (2017). Obtained extracts were filtered through a 0.45 μm polytetrafluoroethylene membrane into a glass vial to remove the insoluble material. The absorption was measured in the wavelength ranges of 239–800 nm with a 3 nm resolution (Jiang et al., 2022). The *MAC* of the BrC fractions in the extracts were calculated as a function of wavelength according to Hecobian et al. (2010):

$$MAC_{offline}(\lambda) = (A_\lambda - A_{700}) \times \frac{V_{extract}}{V_{air} \times L \times C} \times \ln(10) \quad (2)$$

Where A_{700} and A_λ are absorbance values measured by Aqualog, $V_{extract}$ (m^3) is the solvent volume, V_{air} (m^3) is the sampling volume corresponding to the extracted filter, and L is the optical path length of the quartz cuvette (1 cm); C (μg m^{-3}) is the concentration of *ind*-SOA reported by SMPS, assuming that all absorbing *ind*-SOA components were dissolved in methanol.

2.4. Offline analysis by FIGAERO-CIMS and UPLC-PDA-HRMS

The Teflon filters analyzed by FIGAERO-CIMS provide the organic molecular composition of the *ind*-SOA. The instrument and its modes of operation have been described in detail elsewhere (Jiang et al., 2022). Briefly, components of *ind*-SOA sample collected on the Teflon filter were desorbed by a flow of ultra-high-purity (99.9999%) nitrogen gradually heated from 25°C to 200°C over the course of 35 min (Lopez-Hilfiker et al., 2016). The background filter sample was considered as a measurement background. The raw data were analyzed using the toolkit Tofware (v3.1.2, Tofwerk, Thun, Switzerland, and Aerodyne, Billerica) with developed with the Igor Pro software (v7.08, Wavemetrics, Portland, OR). The molecular signals obtained were integrated as thermal desorption chromatograms after background subtraction. During the measurements, the mass resolution of FIGAERO-CIMS was relatively stable with about 4000 m/Δm. Since it was not possible for us to calibrate the sensitivities of all organic molecules, we assume the same sensitivity of 22 cps/ppt for all compounds (Lopez-Hilfiker et al., 2016). As shown in Figure S10, the major compounds ($C_8H_6O_2N_2$, $C_8H_7O_4N$, $C_8H_7O_3N$, and $C_8H_5O_3N$) detected by FIGAERO-CIMS exhibit only one peak in the thermogram and no substantial fragmentation.~~We assume a uniform sensitivity of 22 cps/ppt for all detected compounds (Lopez-Hilfiker et al., 2016).~~

A second quartz filter in each experiment was extracted with 8 mL acetonitrile (Optima LC/MS grade, Fisher Chemical) under sonication. The 8 mL of sample solution was then dried to 2 mL with pure nitrogen. 1 mL of the obtained concentrated solution was used to measure UV-Vis light absorption spectrum by Ocean Optics spectrophotometer. Another 1 mL of the concentrated solution was further dried to 200 uL and then analyzed using an ultra-performance liquid chromatography (UPLC) system (Vanquish) coupled with a photodiode array detector (PDA), an electrospray ionization source (ESI) operated in negative mode and a high-resolution mass spectrometer (HRMS) Q-Exactive HF-X hybrid quadrupole Orbitrap™, all components from Thermo Scientific, Inc. Detailed information of BrC characterization by UPLC-PDA-ESI/HRMS has been published elsewhere (Hettiyadura et al., 2021; Hettiyadura and Laskin, 2022). Briefly, aliquots of ~0.3 μg of *ind*-SOA were injected into the UPLC for analysis. The *ind*-SOA components were separated on a reversed-phase column (Luna C18, 150 × 2 mm, 5 μm particles, 100 Å pores, Phenomenex, Inc.) using a 400 μL min^{-1} binary solvent mixture containing water (A) and acetonitrile (B), with both solvents containing 0.1% (v/v) formic acid. A 36 min LC gradient was programmed as follows: 0–0.5 min at 5% of B, 0.5–26 min at a linear gradient to 100% of B, 26–30.5 min B held at 100%, 30.5–31 min decreased to 5% of B, and 31–36 min held at 5% of B to re-equilibrate the column. The UV-vis absorption spectra of eluted fractions were recorded using the PDA detector over the wavelength range of 300 – 680 nm. Mass spectra were acquired in negative mode over the m/z range of 80 – 1200 Da at a mass resolution of m/Δm = 240 000 at 200 m /z. The raw data were acquired using Xcalibur software (Thermo Scientific) and were further processed using MZmine 2.38 (He et al., 2022). More information on the data analysis is shown in the supplement.

3. RESULTS AND DISCUSSION

3.1. Yield and density of *ind*-SOA

Figure 1 presents the yields and densities of *ind*-SOA measured in three experiments of our study (REF, AS, and AS-NO_2). The REF and AS experiments exhibited the highest yields of *ind*-SOA at 0.45 ± 0.1 and 0.44 ± 0.1, respectively. The AS-NO_2 experiment showed the lowest yield of 0.19 ± 0.02 (Fig. S6 and Table 1). These observations are consistent with previously reported yields of SOA from oxidation of aromatic volatile organic compounds (AVOCs), which tend to show lower yields in the presence of NOx (NO_2 and NO) (Liu et al., 2021; Yang et al., 2022). The AVOCs oxidation products, organic peroxyl radicals (RO_2), mainly react with hydroperoxyl radicals (HO_2) under low-NOx conditions to form oxygenated low volatility species which readily partition into the particle phase, providing growth of the SOA mass (Ng et al., 2007; Xu et al., 2014). However, in the presence of NO_2, gas-phase RO_2 intermediates react with NO_2 to produce fragmented products with higher volatility. These volatile fragmented products remained in the gas phase, inhibiting the particle formation and growth. Notably, a previous study reported a higher yield of *ind*-SOA as 1.3 ± 0.3 under NOx-free conditions with higher initial indole concentrations of 200 ppb (Montoya-Aguilera et al., 2017). In that study, formation of oligomer products of lower volatility was facilitated by higher VOC concentrations, resulting in greater partitioning into particle phase and higher yields. In our study, the highest density of *ind*-SOA was determined as 1.3 ± 0.3 g cm^{-3} in the AS-NO_2 experiment; while the lowest density of 0.8 ± 0.2 g cm^{-3} was observed in the REF experiment. These results suggest that products of large molecular weight were preferentially

formed in *ind*-SOA under conditions of the AS-NO_2 experiment. This observation is consistent with the dominance of a 3-nitroindole (density: 1.4 g cm^{-3}) as a significant component in *ind*-SOA products, accounting for 76% as measured by FIGAERO-CIMS (Fig. 3c). Similarly, Ng et al. (2007) found that the effective density of m-xylene SOA formed in the presence of high-NOx and AS seed particles was 1.5 g cm^{-3}, which was higher than the density of 1.3 g cm^{-3} observed under low-NOx conditions.

3.2. Optical properties of *ind*-SOA

As shown in Figure 2, the indole precursor itself dissolved in methanol absorbs light only at wavelengths below 300 nm. However, all *ind*-SOA samples exhibit appreciable absorption values at longer wavelengths, as illustrated by highest $MAC_{365nm,\ offline}$ value of 4.3 ± 0.4 $m^2\ g^{-1}$ measured in the AS-NO_2 experiment. Additionally, $MAC_{365nm,\ offline}$ values in the AS and REF experiment were comparable but by a factor of five lower, 0.8 ± 0.1 and 0.7 ± 0.1 $m^2\ g^{-1}$, respectively. Consistently, Montoya-Aguilera et al. (2017) also found that *MAC* of *ind*-SOA was ~ 2 m^2g^{-1} at 300 nm and ~ 0.5 m^2g^{-1} at 400 nm. Overall, *MAC* values reported here are higher than those published for secondary BrC generated by atmospheric oxidation of other VOCs, such as 0.29 $m^2\ g^{-1}$ ($MAC_{300–700nm}$) for *ethylbenzene*-SOA formed at high-NOx conditions (Yang et al., 2022), 0.35 $m^2\ g^{-1}$ (MAC_{375nm}) for *pyrrole*-SOA formed by NO_3 radical oxidation (Mayorga et al., 2022), and ≤ 0.01 $m^2\ g^{-1}$ (MAC_{365nm}) for *β-pinene*-SOA (Yang et al., 2022). Therefore, *ind*-SOA is a comparably strong absorbing secondary BrC aerosol.

The highest *MAC* values were detected in the AS-NO_2 experiment, indicating that NO_2 had a significant effect on the formation of BrC chromophores and light-absorption by *ind*-SOA. Lin et al. (2015) also found that NOx affected the production of BrC chromophores in *toluene*-SOA, which were attributed to nitrophenols. Consistently, the online-measured $MAC_{405,\ online}$ values by PAS the AS-NO_2 experiment were also highest values (~3.5 ± 0.4 $m^2\ g^{-1}$), in comparison with $MAC_{405,\ online}$ measured in the REF (0.6 ± 0.2 $m^2\ g^{-1}$) and AS (0.9 ± 0.3 $m^2\ g^{-1}$) experiments (Fig. 2b and S7). The MAC values in REF and AS were similar between online-PAS and offline-Aqualog measurements. However, for the AS-NO_2 experiment, PAS shows higher MAC values at 405 nm than the methanol extract. This difference may be caused by the uncertainties of both measurement techniques, but it may also be attributed to the difference between the absorption measurements of solution and the direct absorption measurement of particles in the air.

3.3. Chemical composition and chromophores of *ind*-SOA

Figure 3 presents the FIGAERO-CIMS mass spectra, O/C ratios, and fractions of $C_xH_yO_zN_{1-2}$ intensities for *ind*-SOA generated in the REF, AS, and AS-NO_2 experiments. In addition, the top 15 products are listed in Table S1, S2, and S3. In the REF and AS experiments (Fig. 3a and 3b), $C_8H_7O_4N$ appears as the major product, accounting for ~10% of all organic compounds detected by FIGAERO-CIMS. $C_8H_7O_3N$ was the second most abundant product accounting for 6%–8% of all organic compounds. $C_8H_5O_3N$ (likely isatoic anhydride) was the third abundant product, accounting for 5%–6% of all organic compounds detected by FIGAERO-CIMS. Interestingly, a new product, not appearing in the REF and AS experiments, was $C_8H_6O_2N_2$ (assigned as 3-nitroindole). Notably, in AS-NO_2 experiment (Fig. 3c), 3-nitroindole significantly dominates *ind*-SOA products with 76% of all organic compounds. Consistently, the 3-nitroindole exhibits the greatest cumulative intensity (1×10^9 A.U.) measured by UPLC-PDA-MS (Fig. 4e).

Furthermore, a dimer product, $C_{16}H_{12}O_4N_4$, accounted for 3.4% of all organic compounds detected by FIGAERO-CIMS. Consistently, high intensities of large-weight fragment ions such as ($C_{13}H_6^+$, $C_5H_6NO_3^+$, and $C_7H_5^+$~~, $C_6H_4^+$, and $C_5H_3^+$~~, etc.) measured by AMS could be fragment~~sed~~ of~~from~~ 3-nitroindole or $C_{16}H_{12}O_4N_4$ (Fig. S8). Due to the high contribution of 3-nitroindole and $C_{16}H_{12}O_4N_4$, *ind*-SOA exhibits a lower O/C ratio (0.32) and a higher mass fraction (93%) of nitrogen-containing molecules in AS-NO_2 experiment relative to the REF and AS experiments (Fig. 3c). Of note, the concentrations of VOC and oxidants in our experiments were more comparable with atmospheric conditions, which is unlike the previous studies discussed here (Montoya-Aguilera et al., 2017). Specifically, Montoya-Aguilera et al. (2017) reported that $C_8H_7O_3N$ and $C_8H_5O_3N$ were the first and second abundant products in *ind*-SOA measured by LC-MS. 3-nitroindole was also identified but at a significantly lower abundance (Montoya-Aguilera et al., 2017). The difference in relative abundance of these products in each study could be due to different experimental conditions and measurement techniques. In our study, lower fractions of products attributed to dimers and trimers were observed, while the previous study of Montoya-Aguilera et al. (2017) performed experiments at an order of magnitude of higher indole concentration (200 ppb) resulting in higher observed fractions of dimers and trimers. A computational study of Xue et al. (2022) found that $C_8H_7O_2N$ [N-(2-formylphenyl)formamide] was an important product from OH radical oxidation of indole. This molecule only accounted for 0.01% – 0.2% of the organic mass in particle phase, but had a higher fraction of 0.1% – 3% in the gas phase measured by FIGAERO-CIMS.

The UPLC-PDA-ESI/HRMS results were used to identify individual BrC chromophores in the *ind*-SOA samples and to assess their contributions to the overall light-absorbing properties of *ind*-SOA formed in the three different experiments of our study. Figure 4 summarizes the BrC molecular characterization results observed for the AS and AS-NO_2 experiments, while those for the REF experiments are included in the supplemental information (Fig. S9). In the *ind*-SOA sample from the AS experiment, the most abundant product, $C_8H_7NO_3$, shows a strong UV-vis feature absorbing in the range of 250–350 nm with ~5×10^4 μAU signal intensity (Fig. 4a). This $C_8H_7NO_3$ product has also been detected as a high intensity $[M-H]^-$ ion (Fig. 4b), consistent with the FIGAERO-CIMS measurements discussed above. Remarkably, this individual $C_8H_7NO_3$ chromophore accounts for 20–35% of overall BrC absorption by the *ind*-SOA generated in the REF and AS experiments (Fig. 4c, S9c, section 6 of the supplement), while its contribution was less prominent in the AS-NO_2 case. The BrC absorption in the AS-NO_2 case is heavily influenced by the 3-nitroindole chromophore, which exhibits a strong absorption band in the 300–400 nm range, resulting in a detected absorbance signal of ~5.5×10^4 μAU (Fig. 4d). Here, the 3-nitroindole chromophore contributes even more significantly, accounting for ~50% of the total BrC absorption (Fig. 4f). Consistent with the FIGAERO-CIMS measurement, 3-nitroindole was detected as the very abundant [M-H]- ion, with a relative abundance approximately two orders of magnitude higher than all other components present in the mixture (Fig. 4e). It follows that NO_2 has a significant effect on the formation of 3-nitroindole, responsible for the BrC absorption in *ind*-SOA.

3.4. Reaction mechanism of the *ind*-SOA formation

The observed differences between *ind*-SOA products formed in different experiments provide insights into potential reaction mechanisms behind their formation, as summarized in Figure 5. The reaction sequences start by abstraction of a hydrogen atom by either OH or NO_3 radicals, likely taking place in position 3 and leading to an indole radical ($C_8H_6N^\bullet$). Consistently, the attack of an electrophile at position 3 in indole generates a carbocation which did not

disturb the aromaticity of the benzene ring (Sundberg, 2012). However, the attack of an electrophile at other positions in indole generates a carbocation which disrupted the aromatic character by delocalizing the positive charge over the benzene ring (Sundberg, 2012). Therefore, position 3 is a preferred site attacked potentially. In the absence of NO_2, $C_8H_6O_2N$ radicals are formed by addition of O_2. Subsequently, the nitrogen-containing ring is opened by reaction with OH radicals leading to the formation of an aldehyde ($C_8H_7O_2N$). In addition, indole can react with O_3 forming $C_8H_7O_3N$ via ozone. Then the nitrogen-containing ring is opened and also leads to formation of $C_8H_7O_2N$. Consistent with this, $C_8H_7O_2N$ was measured by CIMS, accounting for 0.2% of all organic compounds detected by FIGAERO-CIMS. A computational study also predicted $C_8H_7O_2N$ as an important product from OH radical oxidation of indole (Xue et al., 2022). The aldehyde can then undergo further oxidation by OH radicals, forming acids like $C_8H_7O_3N$ and $C_8H_7O_4N$, as also measured by CIMS. This mechanism aligns with the formation of organic acids from the oxidation of aromatic VOC by OH radicals under low-NOx conditions, as reported in previous studies (Montoya-Aguilera et al., 2017; Siemens et al., 2022).

Remarkably, in the presence of NO_2, 3-nitroindole is formed in larger quantities and dominates *ind*-SOA products with 76% of all organic compounds measured by CIMS. This is similar with OH radical induced oxidation of other aromatic compounds like toluene (Lin et al., 2015), naphthalene (Siemens et al., 2022), and pyrrole (Mayorga et al., 2022), where nitro-aromatic compounds are formed in the presence of NO_2. The proposed mechanism is also consistent with the result that 3-nitroindole led to higher light absorption of *ind*-SOA in the presence of NO_2. Therefore, the presence of NO_2 during the formation of *ind*-SOA has a significant effect on the production of 3-nitroindole.

ATMOSPHERIC IMPLICATIONS

This work provides valuable insights into the yield, chemical composition, formation mechanism, and optical properties of *ind*-SOA resulting from oxidation of indole in presence and absence of NO_2. In the absence of NO_2, the dominant products formed are $C_8H_7O_4N$ and $C_8H_7O_3N$. Furthermore, $C_8H_7O_3N$ appears as a major chromophore, contributing 20 – 30% of the total light absorption of *ind*-SOA. However, in presence of NO_2, a significant shift occurs, and 3-nitroindole becomes the dominant compound, comprising up to 76% of the chemical composition measured by CIMS. Interestingly, mass absorption coefficient at 365 nm (MAC_{365}) of *ind*-SOA in the presence of NO_2 is 5 times higher than that of *ind*-SOA formed under each the other investigated conditions. Specifically, 3-nitroindole plays a critical role as the dominant chromophore in *ind*-SOA formed in presence of NO_2, contributing to approximately 50% of the total absorption at 365 nm. These results indicate that the presence of NO_2 during the formation of *ind*-SOA has a substantial impact on the light absorbing properties of aerosol, primarily due to the facilitated formation of 3-nitroindole. Overall, this study complements and expands present understanding of *ind*-SOA formation mechanisms and underscores the significant influence of NO_2 on the chemical composition and the light-absorbing characteristics of *ind*-SOA.

Based on the yields and *MAC* determined in this study, we can estimate the potential absorption of *ind*-SOA formed in the presence of NO_2. Assuming atmospheric indole concentrations of approximately 1.8 during the daytime and 2.6 ppb during the nighttime, as reported for the spring flowering season (Gentner et al., 2014), we can calculate the potential absorption of atmospheric *ind*-SOA ($Abs_{ind\text{-}SOA}$) as follows:

$$Abs_{ind-SOA} = VOC \times Y_{ind-SOA} \times MAC \quad (3)$$

Where VOC is the atmospheric indole concentration (Gentner et al., 2014), Y_{SOA} is the *ind*-SOA yield in the presence of NO_2, and *MAC* is the mass absorption coefficient of *ind*-SOA measured by PAS at 405nm. Using this formula, we estimate the potential $Abs_{ind\text{-}SOA}$ to be approximately 2.3 ± 0.2 Mm^{-1} during the daytime and 3.2 ± 0.3 Mm^{-1} during the nighttime. Notably, $Abs_{ind\text{-}SOA}$ at both times exceeds the total absorption (0.84 ± 0.24 Mm^{-1}) of ambient BrC measured during the summer at a rural background location in Melpitz, Germany (Moschos et al., 2018). Additionally, these calculated absorption values fall within the same range of total light absorption at 365 nm (1.6 ± 0.5 Mm^{-1} in summer and 2.8 ± 1.9 Mm^{-1} in winter) observed for BrC aerosol in an urban area, the city of Karlsruhe (Jiang et al., 2022). These findings highlight that *ind*-SOA can have a significant impact on climate and air quality, particularly, during the spring season or downwind of larger animal husbandries and maize fields. However, this may be limited to regions with corresponding emissions of both NO_2 and indole. The potential impact should be studied in atmospheric transport models using realistic emission scenarios.

Data availability

The data related to this article is accessible at KIT open data (link/DOI, will be completed). Data are available upon request to the corresponding author.

Author contributions

FJ operated AMS and FIGAERO-CIMS, took the filter samples, analyzed the filters by CIMS, UPLC-PDA-ESI/HRMS, UV-visible spectrometer, and Aqualog in the laboratory, performed the CIMS and UPLC-PDA-ESI/HRMS data analysis, produced all figures, and drafted the paper. KS operated UPLC-PDA-ESI/HRMS, UV-visible spectrometer, and provided guidance for the associated tasks of data analysis and presentation. CL operated PAS and analyzed the PAS data. YL operated PTR-ToF-MS and analyzed the PTR-ToF-MS data. YG collected the filter samples. AM guided HRMS data analysis. TL gave general advice and comments for this paper. AL oversaw the UPLC-PDA-ESI/MS measurement and data interpretation. HS operated the AIDA simulation chamber, oversaw data analysis and interpretation. All authors provided suggestions for the data analysis, interpretation, and discussion, and edited manuscript.

Competing interests

At least one of the co-authors is a member of the editorial board of Atmospheric Chemistry and Physics. The authors declare that they have no conflict of interest.

ACKNOWLEDGMENTS

The authors gratefully thank the staff at IMK-AAF and KIT-IGG for providing substantial technical support. Feng Jiang thanks for the support from the China Scholarship Council (CSC) and KIT Grace. KS and AL acknowledge support from the US National Science Foundation award AGS-20239985.

REFERENCES

Andreae, M. O., and Gelencser, A.: Black carbon or brown carbon? The nature of light-absorbing carbonaceous aerosols, Atmospheric Chemistry and Physics, 6, 3131-3148, 10.5194/acp-6-3131-2006, 2006.

Atkinson, R., Tuazon, E. C., Arey, J., and Aschmann, S. M.: Atmospheric and Indoor Chemistry of Gas-phase Indole, Quinoline, and Isoquinoline, Atmospheric Environment, 29, 3423-3432, 10.1016/1352-2310(95)00103-6, 1995.

Baboomian, V. J., He, Q., Montoya-Aguilera, J., Ali, N., Fleming, L. T., Lin, P., Laskin, A., Laskin, J., Rudich, Y., and Nizkorodov, S. A.: Light absorption and scattering properties of indole secondary organic aerosol prepared under various oxidant and relative humidity conditions, Aerosol Science and Technology, 1-14, 10.1080/02786826.2023.2193235, 2023.

Bloss, C., Wagner, V., Jenkin, M. E., Volkamer, R., Bloss, W. J., Lee, J. D., Heard, D. E., Wirtz, K., Martin-Reviejo, M., Rea, G., Wenger, J. C., and Pilling, M. J.: Development of a detailed chemical mechanism (MCMv3.1) for the atmospheric oxidation of aromatic hydrocarbons, Atmos. Chem. Phys., 5, 641–664, https://doi.org/10.5194/acp-5-641-2005, 2005.

Erb, M., Veyrat, N., Robert, C. A. M., Xu, H., Frey, M., Ton, J., and Turlings, T. C. J.: Indole is an essential herbivore-induced volatile priming signal in maize, Nature Communications, 6, 10.1038/ncomms7273, 2015.

Feng, Y., Ramanathan, V., and Kotamarthi, V. R.: Brown carbon: a significant atmospheric absorber of solar radiation?, Atmospheric Chemistry and Physics, 13, 8607-8621, 10.5194/acp-13-8607-2013, 2013.

Gao, L., Song, J., Mohr, C., Huang, W., Vallon, M., Jiang, F., Leisner, T., and Saathoff, H.: Kinetics, SOA yields, and chemical composition of secondary organic aerosol from β-caryophyllene ozonolysis with and without nitrogen oxides between 213 and 313 K, Atmos. Chem. Phys., 22, 6001-6020, 10.5194/acp-22-6001-2022, 2022.

Gentner, D. R., Ormeno, E., Fares, S., Ford, T. B., Weber, R., Park, J. H., Brioude, J., Angevine, W. M., Karlik, J. F., and Goldstein, A. H.: Emissions of terpenoids, benzenoids, and other biogenic gas-phase organic compounds from agricultural crops and their potential implications for air quality, Atmospheric Chemistry and Physics, 14, 5393-5413, 10.5194/acp-14-5393-2014, 2014.

Hallquist, M., Wenger, J. C., Baltensperger, U., Rudich, Y., Simpson, D., Claeys, M., Dommen, J., Donahue, N. M., George, C., Goldstein, A. H., Hamilton, J. F., Herrmann, H., Hoffmann, T., Iinuma, Y., Jang, M., Jenkin, M. E., Jimenez, J. L., Kiendler-Scharr, A., Maenhaut, W., McFiggans, G., Mentel, T. F., Monod, A., Prevot, A. S. H., Seinfeld, J. H., Surratt, J. D., Szmigielski, R., and Wildt, J.: The formation, properties and impact of secondary organic aerosol: current and emerging issues, Atmospheric Chemistry and Physics, 9, 5155-5236, 10.5194/acp-9-5155-2009, 2009.

He, Q. F., Li, C. L., Siemens, K., Morales, A. C., Hettiyadura, A. P. S., Laskin, A., and Rudich, Y.: Optical Properties of Secondary Organic Aerosol Produced by Photooxidation of Naphthalene under NOx Condition, Environ. Sci. Technol., 56, 4816-4827, 10.1021/acs.est.1c07328, 2022.

Hecobian, A., Zhang, X., Zheng, M., Frank, N., Edgerton, E. S., and Weber, R. J.: Water-Soluble Organic Aerosol material and the light-absorption characteristics of aqueous extracts measured over the Southeastern United States, Atmospheric Chemistry and Physics, 10, 5965-5977, 10.5194/acp-10-5965-2010, 2010.

Hettiyadura, A. P. S., Garcia, V., Li, C., West, C. P., Tomlin, J., He, Q., Rudich, Y., and Laskin, A.: Chemical Composition and Molecular-Specific Optical Properties of Atmospheric Brown Carbon Associated with Biomass Burning, Environ. Sci. Technol., 10.1021/acs.est.0c05883, 2021.

Hettiyadura, A. P. S., and Laskin, A.: Quantitative analysis of polycyclic aromatic hydrocarbons using high-performance liquid chromatography-photodiode array-high-resolution mass spectrometric detection platform coupled to electrospray and atmospheric pressure photoionization sources, Journal of Mass Spectrometry, 57, 10.1002/jms.4804, 2022.

Jiang, F., Song, J., Bauer, J., Gao, L., Vallon, M., Gebhardt, R., Leisner, T., Norra, S., and Saathoff, H.: Chromophores and chemical composition of brown carbon characterized at an urban kerbside by excitation–emission spectroscopy and mass spectrometry, Atmos. Chem. Phys., 22, 14971-14986, 10.5194/acp-22-14971-2022, 2022.

Jiang, H. H., Frie, A. L., Lavi, A., Chen, J. Y., Zhang, H. F., Bahreini, R., and Lin, Y. H.: Brown Carbon Formation from Nighttime Chemistry of Unsaturated Heterocyclic Volatile Organic Compounds, Environmental Science & Technology Letters, 6, 184-190, 10.1021/acs.estlett.9b00017, 2019.

Kostenidou, E., Pathak, R. K., and Pandis, S. N.: An algorithm for the calculation of secondary organic aerosol density combining AMS and SMPS data, Aerosol Science and Technology, 41, 1002-1010, 10.1080/02786820701666270, 2007.

Lambe, A. T., Zhang, J. Y., Sage, A. M., and Donahue, N. M.: Controlled OH radical production via ozone-alkene reactions for use in aerosol aging studies, Environ. Sci. Technol., 41, 2357-2363, 10.1021/es061878e, 2007.

Laskin, A., Smith, J. S., and Laskin, J.: Molecular Characterization of Nitrogen-Containing Organic Compounds in Biomass Burning Aerosols Using High-Resolution Mass Spectrometry, Environ. Sci. Technol., 43, 3764-3771, 10.1021/es803456n, 2009.

Laskin, A., Laskin, J., and Nizkorodov, S. A.: Chemistry of Atmospheric Brown Carbon, Chemical Reviews, 115, 4335-4382, 10.1021/cr5006167, 2015.

Laskin, J., Laskin, A., Nizkorodov, S. A., Roach, P., Eckert, P., Gilles, M. K., Wang, B. B., Lee, H. J., and Hu, Q. C.: Molecular Selectivity of Brown Carbon Chromophores, Environ. Sci. Technol., 48, 12047-12055, 10.1021/es503432r, 2014.

Li, C. L., Windwer, E., Fang, Z., Nissenbaum, D., and Rudich, Y.: Correcting micro-aethalometer absorption measurements for brown carbon aerosol, Science of the Total Environment, 777, 10.1016/j.scitotenv.2021.146143, 2021a.

Li, Y. X., Zhao, J. Y., Wang, Y., Seinfeld, J. H., and Zhang, R. Y.: Multigeneration Production of Secondary Organic Aerosol from Toluene Photooxidation, Environ. Sci. Technol., 55, 8592-8603, 10.1021/acs.est.1c02026, 2021b.

Lin, P., Liu, J., Shilling, J. E., Kathmann, S. M., Laskin, J., and Laskin, A.: Molecular characterization of brown carbon (BrC) chromophores in secondary organic aerosol generated from photo-oxidation of toluene, Physical Chemistry Chemical Physics, 17, 23312-23325, 10.1039/c5cp02563j, 2015.

Linke, C., Ibrahim, I., Schleicher, N., Hitzenberger, R., Andreae, M. O., Leisner, T., and Schnaiter, M.: A novel single-cavity three-wavelength photoacoustic spectrometer for atmospheric aerosol research, Atmospheric Measurement Techniques, 9, 5331-5346, 10.5194/amt-9-5331-2016, 2016.

Liu, S., Huang, D., Wang, Y., Zhang, S., Liu, X., Wu, C., Du, W., and Wang, G.: Synergetic effects of NH3 and NOx on the production and optical absorption of secondary organic aerosol formation from toluene photooxidation, Atmos. Chem. Phys., 21, 17759-17773, 10.5194/acp-21-17759-2021, 2021.

Lopez-Hilfiker, F. D., Iyer, S., Mohr, C., Lee, B. H., D'Ambro, E. L., Kurten, T., and Thornton, J. A.: Constraining the sensitivity of iodide adduct chemical ionization mass spectrometry to multifunctional organic molecules using the collision limit and thermodynamic stability of iodide ion adducts, Atmospheric Measurement Techniques, 9, 1505-1512, 10.5194/amt-9-1505-2016, 2016.

Mayorga, R., Chen, K., Raeofy, N., Woods, M., Lum, M., Zhao, Z., Zhang, W., Bahreini, R., Lin, Y.-H., and Zhang, H.: Chemical Structure Regulates the Formation of Secondary Organic Aerosol and Brown Carbon in Nitrate Radical Oxidation of Pyrroles and Methylpyrroles, Environ. Sci. Technol., 10.1021/acs.est.2c02345, 2022.

Misztal, P. K., Hewitt, C. N., Wildt, J., Blande, J. D., Eller, A. S. D., Fares, S., Gentner, D. R., Gilman, J. B., Graus, M., Greenberg, J., Guenther, A. B., Hansel, A., Harley, P., Huang, M., Jardine, K., Karl, T., Kaser, L., Keutsch, F. N., Kiendler-Scharr, A., Kleist, E., Lerner, B. M., Li, T., Mak, J., Nolscher, A. C., Schnitzhofer, R., Sinha, V., Thornton, B., Warneke, C., Wegener, F., Werner, C., Williams, J., Worton, D. R., Yassaa, N., and Goldstein, A. H.: Atmospheric benzenoid emissions from plants rival those from fossil fuels, Scientific Reports, 5, 10.1038/srep12064, 2015.

Moise, T., Flores, J. M., and Rudich, Y.: Optical Properties of Secondary Organic Aerosols and Their Changes by Chemical Processes, Chemical Reviews, 115, 4400-4439, 10.1021/cr5005259, 2015.

Montoya-Aguilera, J., Horne, J. R., Hinks, M. L., Fleming, L. T., Perraud, V., Lin, P., Laskin, A., Laskin, J., Dabdub, D., and Nizkorodov, S. A.: Secondary organic aerosol from atmospheric photooxidation of indole, Atmospheric Chemistry and Physics, 17, 11605-11621, 10.5194/acp-17-11605-2017, 2017.

Moschos, V., Kumar, N. K., Daellenbach, K. R., Baltensperger, U., Prevot, A. S. H., and El Haddad, I.: Source Apportionment of Brown Carbon Absorption by Coupling Ultraviolet-Visible Spectroscopy with Aerosol Mass Spectrometry, Environmental Science & Technology Letters, 5, 302-+, 10.1021/acs.estlett.8b00118, 2018.

Ng, N. L., Kroll, J. H., Chan, A. W. H., Chhabra, P. S., Flagan, R. C., and Seinfeld, J. H.: Secondary organic aerosol formation from m-xylene, toluene, and benzene, Atmospheric Chemistry and Physics, 7, 3909-3922, 10.5194/acp-7-3909-2007, 2007.

Saathoff, H., Naumann, K. H., Mohler, O., Jonsson, A. M., Hallquist, M., Kiendler-Scharr, A., Mentel, T. F., Tillmann, R., and Schurath, U.: Temperature dependence of yields of secondary organic aerosols from the ozonolysis of alpha-pinene and limonene, Atmospheric Chemistry and Physics, 9, 1551-1577, 10.5194/acp-9-1551-2009, 2009.

Salo, K., Hallquist, M., Jonsson, A. M., Saathoff, H., Naumann, K. H., Spindler, C., Tillmann, R., Fuchs, H., Bohn, B., Rubach, F., Mentel, T. F., Muller, L., Reinnig, M., Hoffmann, T., and Donahue, N. M.: Volatility of secondary organic aerosol during OH radical induced ageing, Atmospheric Chemistry and Physics, 11, 11055-11067, 10.5194/acp-11-11055-2011, 2011.

Shrivastava, M., Cappa, C. D., Fan, J. W., Goldstein, A. H., Guenther, A. B., Jimenez, J. L., Kuang, C., Laskin, A., Martin, S. T., Ng, N. L., Petaja, T., Pierce, J. R., Rasch, P. J., Roldin, P., Seinfeld, J. H., Shilling, J., Smith, J. N., Thornton, J. A., Volkamer, R., Wang, J., Worsnop, D. R., Zaveri, R. A., Zelenyuk, A., and Zhang, Q.: Recent advances in understanding secondary organic aerosol: Implications for global climate forcing, Reviews of Geophysics, 55, 509-559, 10.1002/2016rg000540, 2017.

Siemens, K., Morales, A., He, Q., Li, C., Hettiyadura, A. P. S., Rudich, Y., and Laskin, A.: Molecular Analysis of Secondary Brown Carbon Produced from the Photooxidation of Naphthalene, Environ. Sci. Technol., 56, 3340-3353, 10.1021/acs.est.1c03135, 2022.

Skoczek, A., Piesik, D., Wenda-Piesik, A., Buszewski, B., Bocianowski, J., and Wawrzyniak, M.: Volatile organic compounds released by maize following herbivory or insect extract application and communication between plants, Journal of Applied Entomology, 141, 630-643, 10.1111/jen.12367, 2017.

Sundberg, R.: The chemistry of indoles, Elsevier, 2012.

Xie, M., Chen, X., Hays, M. D., Lewandowski, M., Offenberg, J., Kleindienst, T. E., and Holder, A. L.: Light Absorption of Secondary Organic Aerosol: Composition and Contribution of Nitroaromatic Compounds, Environ. Sci. Technol., 51, 11607-11616, 10.1021/acs.est.7b03263, 2017.

Xu, L., Kollman, M. S., Song, C., Shilling, J. E., and Ng, N. L.: Effects of NOx on the Volatility of Secondary Organic Aerosol from Isoprene Photooxidation, Environ. Sci. Technol., 48, 2253-2262, 10.1021/es404842g, 2014.

Xue, J., Ma, F., Elm, J., Chen, J., and Xie, H. B.: Atmospheric Oxidation Mechanism and Kinetics of Indole Initiated by ·OH and ·Cl: A Computational Study, Atmos. Chem. Phys. 2022, 1-23, 10.5194/acp-2022-88, 2022.

Yang, Z., Tsona, N. T., George, C., and Du, L.: Nitrogen-Containing Compounds Enhance Light Absorption of Aromatic-Derived Brown Carbon, Environ. Sci. Technol., 10.1021/acs.est.1c08794, 2022.

Yu, F., and Luo, G.: Modeling of gaseous methylamines in the global atmosphere: impacts of oxidation and aerosol uptake, Atmospheric Chemistry and Physics, 14, 12455-12464, 10.5194/acp-14-12455-2014, 2014.

Yuan, B., Coggon, M. M., Koss, A. R., Warneke, C., Eilerman, S., Peischl, J., Aikin, K. C., Ryerson, T. B., and de Gouw, J. A.: Emissions of volatile organic compounds (VOCs) from concentrated animal feeding operations (CAFOs): chemical compositions and separation of sources, Atmospheric Chemistry and Physics, 17, 4945-4956, 10.5194/acp-17-4945-2017, 2017.

Zeng, L., Dibb, J., Scheuer, E., Katich, J. M., Schwarz, J. P., Bourgeois, I., Peischl, J., Ryerson, T., Warneke, C., Perring, A. E., Diskin, G. S., DiGangi, J. P., Nowak, J. B., Moore, R. H., Wiggins, E. B., Pagonis, D., Guo, H., Campuzano-Jost, P., Jimenez, J. L., Xu, L., and Weber, R. J.: Characteristics and Evolution of Brown Carbon in Western United States Wildfires, Atmos. Chem. Phys. 2022, 1-45, 10.5194/acp-2022-70, 2022.

Zeng, L. T., Zhou, Y., Gui, J. D., Fu, X. M., Mei, X., Zhen, Y. P., Ye, T. X., Du, B., Dong, F., Watanabe, N., and Yang, Z. Y.: Formation of Volatile Tea Constituent Indole During the Oolong Tea Manufacturing Process, Journal of Agricultural and Food Chemistry, 64, 5011-5019, 10.1021/acs.jafc.6b01742, 2016.

Table 1. Summary of indole SOA experimental conditions.

Experiment ID	Indole (ppb)	NO_2 (ppb)	$(NH_4)_2SO_4$ seed	RH (%)	Temperature (°C)	SOA density (g cm^{-3})	$Yield_{SOA}$
REF	20.5	–	–	29	30	0.8 ± 0.2	0.45 ± 0.1
AS	24.5	–	√	28	30	0.9 ± 0.2	0.44 ± 0.1
AS-NO_2	18.6	60	√	29	30	1.3 ± 0.3	0.19 ± 0.02
~~Experiment ID~~	~~Indole (ppb)~~	~~NO_2 (ppb)~~	~~$(NH_4)_2SO_4$ seed~~	~~RH (%)~~	~~Temperature (°C)~~	~~SOA density (g cm^{-3})~~	~~$Yield_{SOA}$~~
~~REF~~	~~20.5~~	~~–~~	~~–~~	~~29~~	~~30~~	~~0.8 ± 0.2~~	~~0.45 ± 0.1~~
~~AS~~	~~24.5~~	~~–~~	~~√~~	~~28~~	~~30~~	~~0.9 ± 0.2~~	~~0.44 ± 0.1~~
~~AS-NO_2~~	~~18.6~~	~~60~~	~~√~~	~~29~~	~~30~~	~~1.3 ± 0.3~~	~~0.19 ± 0.02~~

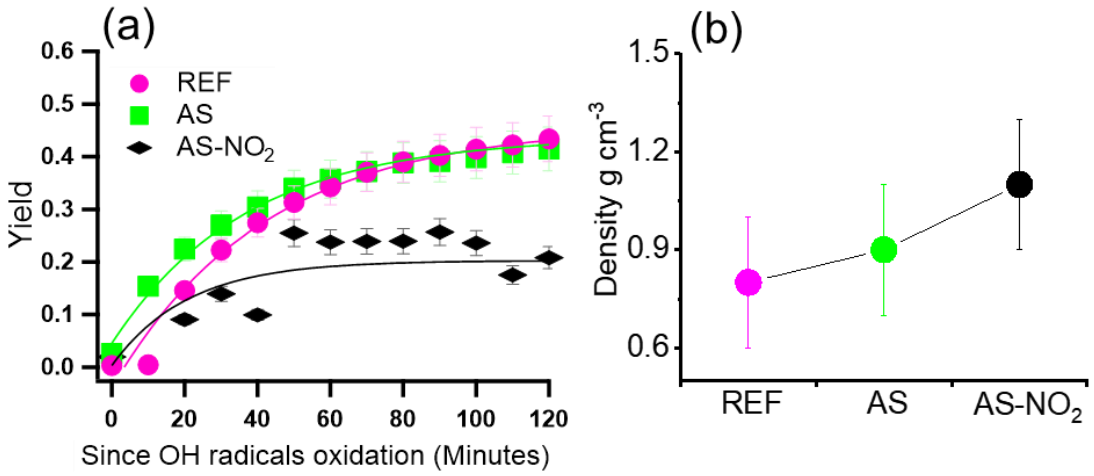

Figure 1. Evolution (a) of indole SOA yield with OH radical oxidation time and density (b) of indole SOA. The lines (Figure 1a) were fitted by exponential functions. REF (pink), AS (green), and AS-NO_2 (black). The yields were calculated under stable periods for one hour.

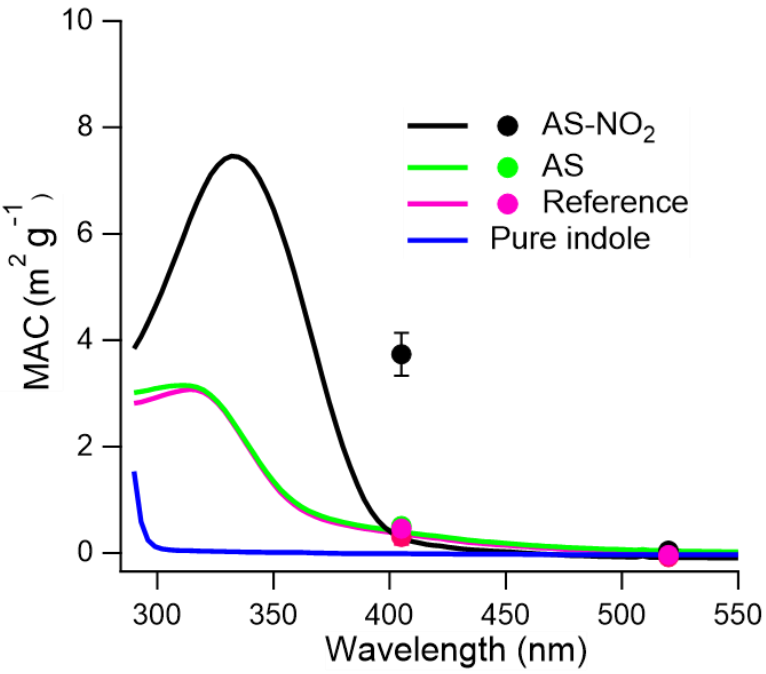

505 **Figure 2.** ***MAC*** **of methanol-soluble between 290–550 nm from Aqualog measurements (lines). The** ***MAC*** **values of BrC aerosol particles at 405 nm and 520 nm measured by photoacoustic spectroscopy (circles). AS-NO$_2$ (black), AS (green), REF (pink), and pure indole (blue).**

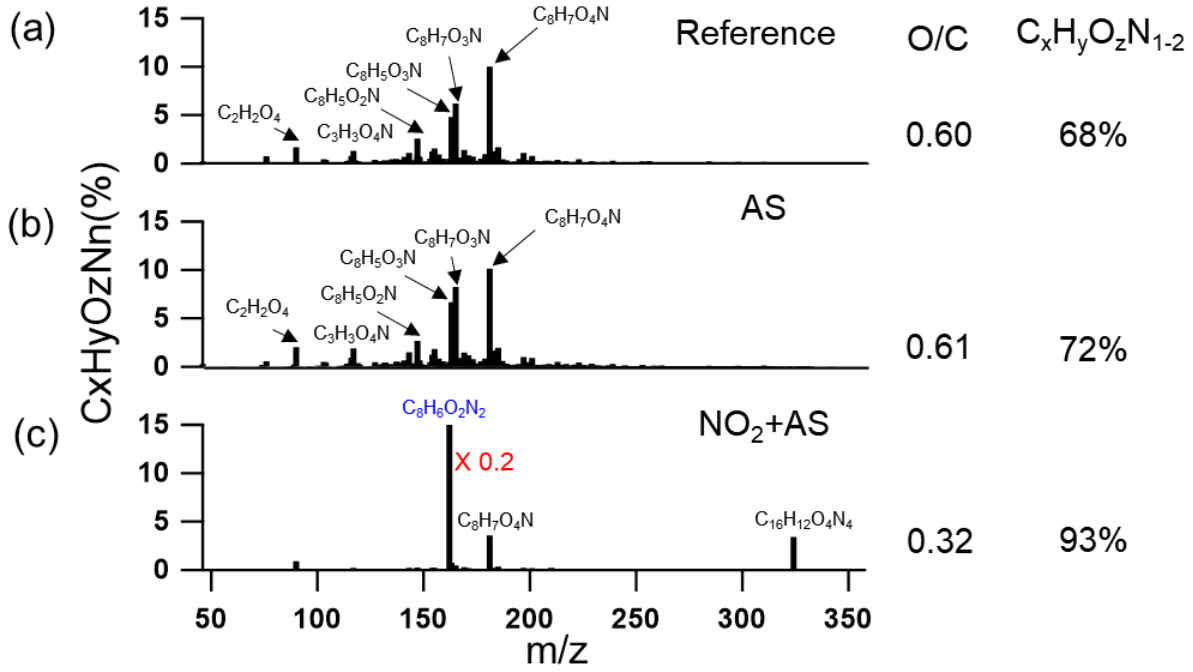

Figure 3. CIMS mass spectra of particle-phase *ind*-SOA (products generated in the REF, AS, and AS-NO_2 experiments). The CI source employs reactions of I- ions, which convert analyte molecules into [M+I]- ions. Legends above MS features correspond to neutral molecules. The blue legend indicates the most abundant features of $C_8H_6O_2N_2$. The mass fraction of $C_8H_6O_2N_2$ was multiplied by 0.2 since the fraction was too high. O/C ratios were calculated based on intensity-weighted sum of all compounds. TThe Y-axis scale shows the fraction of $C_xH_yO_zN_{1-2}$ of the total ion intensity is shown on the right..

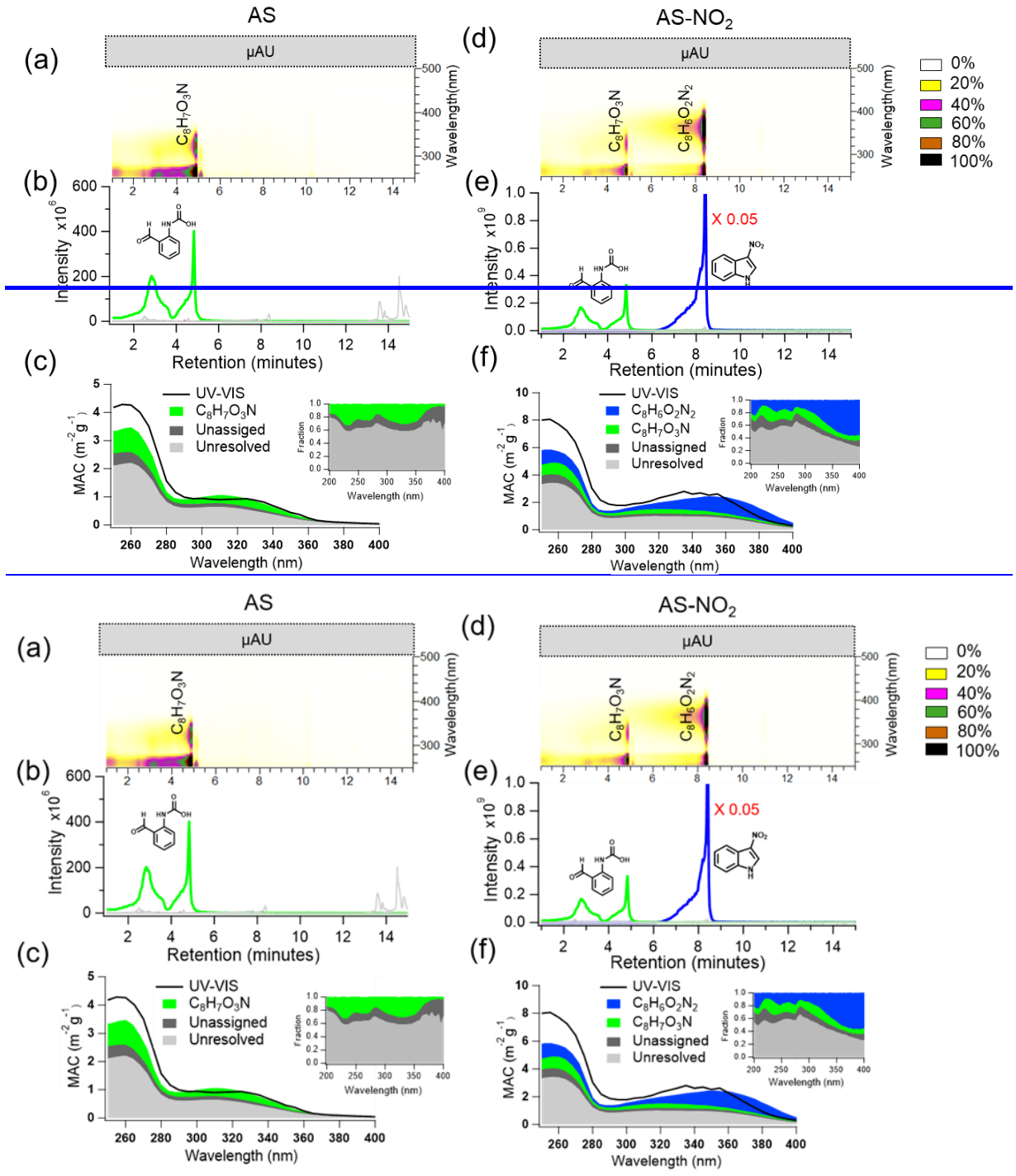

Figure 4. Molecular characteristics of individual components identified in the *ind*-SOA formed under AS and AS-NO_2 conditions. Panels (a, d) are the normalized UPLC-PDA chromatograms color-mapped based on relative absorbance, with major chromophores labeled as neutral species. Panels (b, e) show a compilation of the selected extracted ion chromatograms (EICs) along with proposed molecular structures of the most abundant peaks. Panels (c, fd) illustrate the *MAC* calculated from UV-visible spectrometer and PDA measurements. The PDA signal is grouped by contribution from unresolved chromophores (grey), unassigned chromophores (blackred), $C_8H_7NO_3$ (green), and $C_8H_6N_2O_2$ (blue).

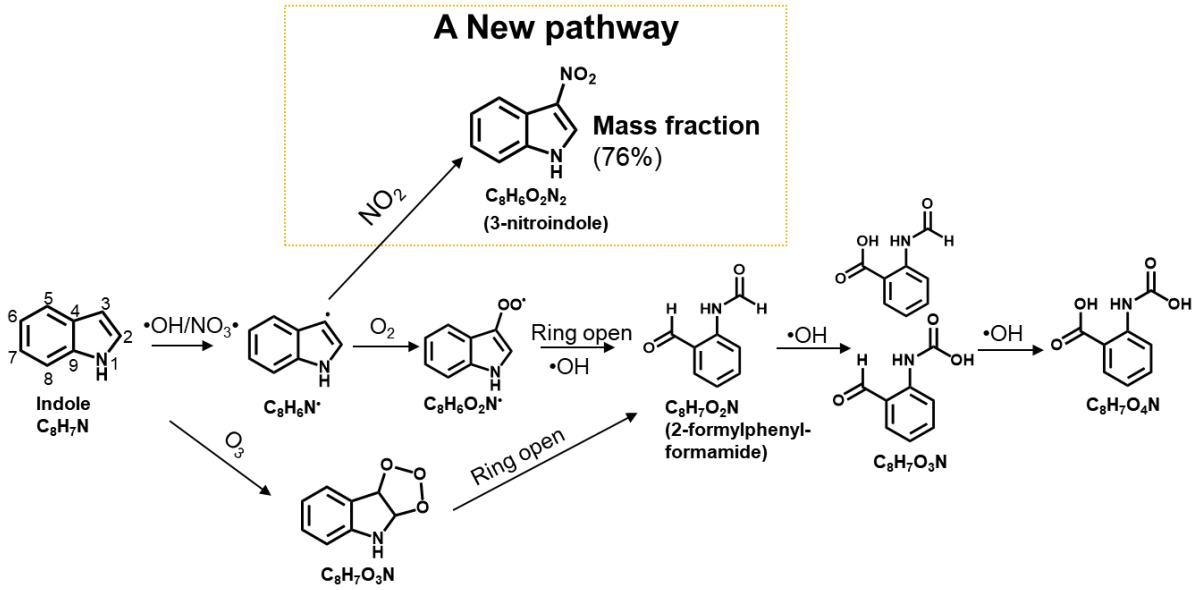

525

Figure 5. Proposed chemical reaction pathways leading to the major components of indole SOA observed in the particle phase including an efficient reaction with NO_2 to 3-nitroindole.

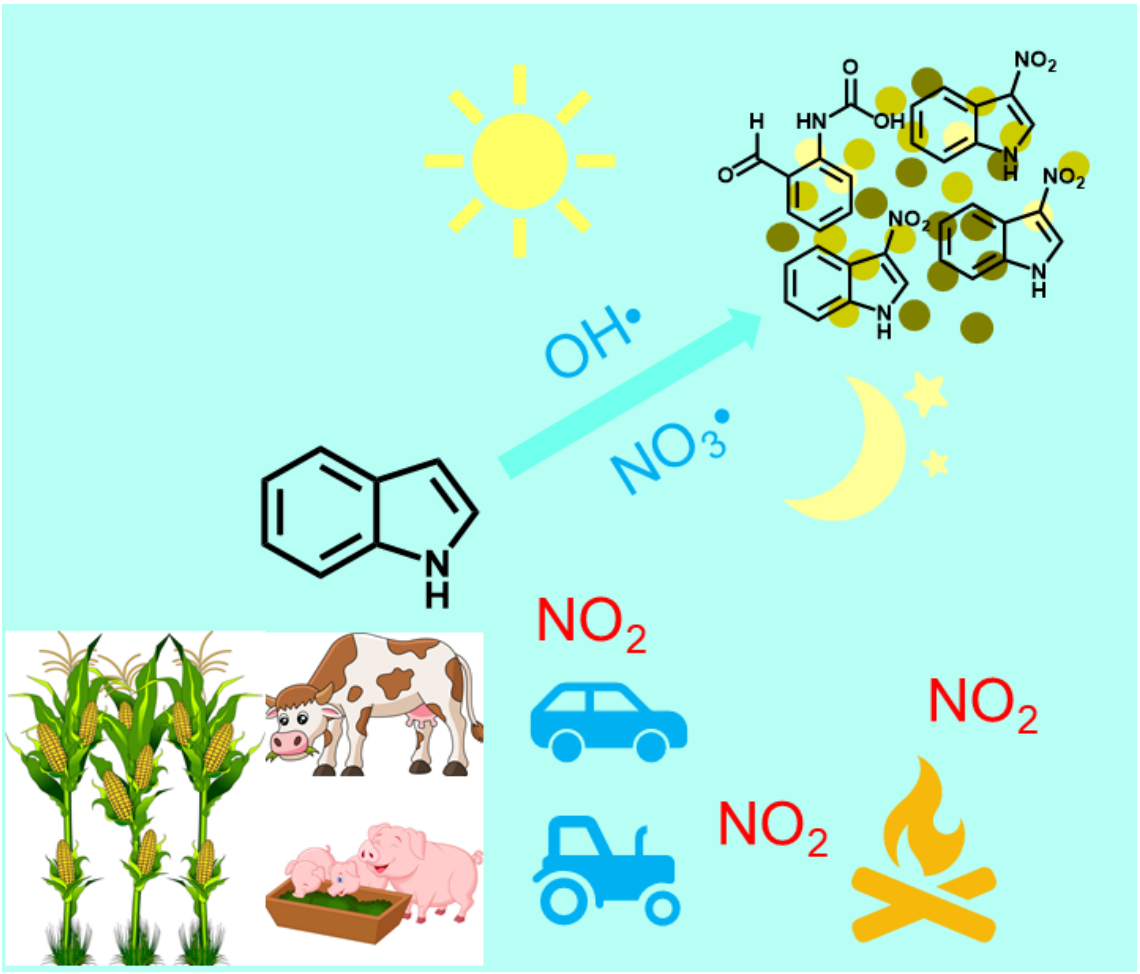

Figure 6. A conceptual picture shows the brown carbon from the oxidation of indole emitted from maize and animal husbandry.